THE JOURNAL OF PHYSICAL CHEMISTRY LETTERS
A JOURNAL OF THE AMERICAN CHEMICAL SOCIETY

pubs.acs.org/JPCL

Letter

Theoretical and Experimental Investigation of the Electronic Propensity Rule: A Linear Relationship between Radiative and Nonradiative Decay Rates of Molecules

Ying Zhang, Heyuan Liu, and Yuxiang Weng*

Cite This: *J. Phys. Chem. Lett.* 2023, 14, 4151−4157

Read Online

ACCESS | Metrics & More | Article Recommendations | Supporting Information

ABSTRACT: The electronic propensity rule, which suggests a proportional relationship between radiative and nonradiative electronic coupling elements in fluorescent molecules, has been postulated for some time. Despite its potential significance, the rule has not been rigorously derived and experimentally validated. In this work, we draw upon the theoretical framework established by Schuurmans et al. for the relation between the radiative and nonradiative electronic coupling elements of the rare earth metal in the crystal at low temperature and extend their approach to the fluorescent molecules under external electric field perturbation at a fixed energy gap and varied temperatures, with a further single-electron approximation (Schuurmans, M. F. H., et al. *Physica B & C* **1984**, *123*, 131−155). We obtained a linear relation between the radiative decay rates and nonradiative decay rates for internal conversion, which is verified by experimental data from two types of dextran−dye complexes and the light-harvesting antenna complex in photosynthetic bacteria.

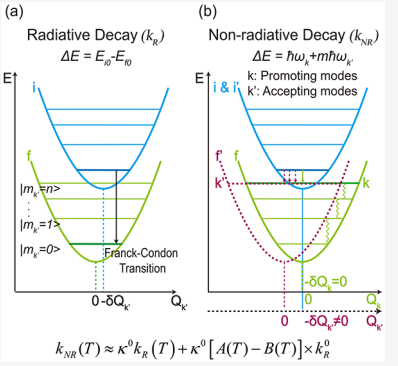

The rational design of fluorescent molecules is a fundamental scientific question with numerous applications, ranging from molecular biological imaging to organic light-emitting diodes and laser applications.[1−4] The intense fluorescence of these molecules arises from the interplay of two rate processes of electronic relaxations: radiative and nonradiative transitions. Recently, the relationship between the two rates of fluorescent molecules has been intensively discussed with the commencement of the field known as aggregation-induced emission (AIE).[5−7]

Radiative deactivation channels involve the emission of a photon with energy equal to or less than the excitation energy, whereas nonradiative channels transfer excitation energy to the vibrational levels without any photon emission. This Letter draws attention to the intramolecular nonradiative processes, specifically internal conversion (IC).[4] The radiative decay rate (k_R)[8,9] and nonradiative decay rate (k_{NR})[10−15] have been subjects of intense theoretical discussion. Radiative decay is typically considered to be an electronic relaxation process that involves the emission of a photon without any phonons participating in the electronic transition. As such, k_R is primarily determined by the electronic structures of molecules in terms of the electronic coupling element. In contrast, k_{NR} is a product of two factors: the electronic coupling element resulting from high-frequency promoting modes and the Franck−Condon factor constituted by accepting modes. A majority of discussions regarding nonradiative decay rates have focused on the Franck−Condon factor, leading to the well-known energy gap law.[13,16,17]

Principally, the interaction with the radiation field determines the properties of the prepared excited states and thus the electronic coupling terms of the molecules.[18] Based on this idea, an electronic propensity rule, independent of the Franck−Condon principle, is proposed by Siebrand et al.[18] This rule indicates that in a series of related molecules or comparable states of the same molecule when the radiative rate constants increase, the rates of competing nonradiative decay processes would increase correspondingly.[18,19] Moreover, Schuurmans et al. provided a detailed derivation on the ratio between k_R and k_{NR} for rare earth ions under conditions of weak electron−phonon coupling at zero K.[20]

In this Letter, we extend the derivation of Schuurmans et al. to fluorescent molecules under external electric field perturbation at a fixed energy gap and varied temperatures, using the single-electron approximation.[20] We obtain a general linear relation between k_R and k_{NR} when changing the local electric field around the molecules. This linear relationship is further verified by experimental results of dextran−dye complexes and the light-harvesting antenna complexes (LH2) of photosynthetic bacteria. The linear relation between k_R and k_{NR} can be helpful in experiments where the fluorescence

Received: March 15, 2023
Accepted: April 21, 2023

https://doi.org/10.1021/acs.jpclett.3c00697
J. Phys. Chem. Lett. 2023, 14, 4151−4157

quantum yield (Φ) cannot be directly measured, such as in scattering or self-absorption systems. In such cases, we can determine k_R and k_{NR} under nonscattering and dilute conditions, establishing the linear relation for the molecules. With the known linear relation, Φ in scattering or self-absorption systems can be determined by the measured fluorescence lifetime.

We restrict our attention to cases where the displacements of the potential energy curves in an electronic transition are small, signifying weak electron−phonon coupling, and where the distortions of the potential energy surfaces can be ignored. In such scenarios, the Born−Oppenheimer approximation naturally holds, which assumes that the electronic and nuclear motions are separable. The wave functions (Ψ) can then be expressed as a product of electronic (ϕ) and vibrational (χ) wave functions, i.e. $\Psi_{lm}(\boldsymbol{r},\boldsymbol{R}) = \phi_l(\boldsymbol{r},\boldsymbol{R})\chi_{m(l)}(\boldsymbol{R})$.[16,20] Here, $\boldsymbol{r}$ and $\boldsymbol{R}$ denote the electron and nuclei coordinates, respectively, l and m are the quantum numbers for the electronic and vibrational states, and the corresponding eigenenergy will be represented by E_{lm}. Under the harmonic approximation, the vibrational wave function can be written as $\chi_{m_{(l)}} = \prod_{k=1}^{3N} X_{m_{k;l}}(Q_{k;l})$, where k stands for normal modes and Q stands for normal coordinates. The vibrational eigenfunctions $X_{m_{k;l}}(Q_{k;l})$ can be expressed by the Hermite polynomial H_{m_k}, where m_k is the quantum number of the kth mode (see SI-1).

In the context of weak electron−phonon coupling, Fermi's golden rule is frequently utilized to characterize both the radiative and internal nonradiative decay rates in large molecules.[14,21] For simplicity, we will consider the low-temperature case, indicating that only the lowest vibrational state of the upper energy state is occupied, and then we have

$$k(i0 \to fm) = \frac{2\pi}{\hbar}\sum_m \left|\langle\phi_f|H|\phi_i\rangle\left\langle\prod_k X_{m_{k;f}}(Q_k)|H|\prod_{k'} X_{0_{k';i}}(Q_{k'})\right\rangle\right|^2 \times \delta(E_{i0} - E_{fmk}) \quad (1)$$

where i and f refer to the initial and final electronic states and $m' = 0$ and m are the quantum numbers of the vibrational states in the initial and final electronic states, respectively. k' also stands for normal modes, and H is the Hamiltonian of the electron−nuclei interacting system. The transition matrix elements are divided into two factors: the electronic part $\langle\phi_f|H|\phi_i\rangle$ and the vibrational part $\langle X_{m_{kf}}(Q_k)|H|X_{0_{k'i}}(Q_{k'})\rangle$.

The radiative decay rate (k_R) is typically calculated using either the zero-phonon absorption line[20] or the spontaneous emission equation,[5,22] both of which emphasize the electronic part of the transition. Meanwhile, the Franck−Condon factor is considered to have a value of 1 for the 0−0 transition. Thus, k_R can be simplified to[8,9,20] (see SI-2)

$$k_R(i \to f) \simeq \frac{4|J|^2}{3\hbar^4 c^3}\Delta E^3 \quad (2)$$

where

$$J = \langle\phi_f|\boldsymbol{\mu}|\phi_i\rangle_e \quad (3)$$

Here, $\boldsymbol{\mu}$ is the electric dipole moment with summation running over all electrons ($\sum_e e\mathbf{r}_e$) and ΔE is the energy difference given by $\Delta E = E_i - E_f$.

The expression for the nonradiative decay rate (k_{NR}) similar to eq 2 is given as

$$k_{NR} = \frac{\pi\eta\hbar^2}{Md}\left(\sum_{k_p=1}^{p}|J_{if}^{k_p}|^2\omega_{k_p}\right)\exp(\gamma(\Delta E + \delta E)) \quad (4)$$

where the electronic part of k_{NR} in the Condon approximation is defined as[20]

$$J_{if}^k = \left\langle\phi_f\left|\frac{\partial}{\partial Q_k}\right|\phi_i\right\rangle_e \quad (5)$$

The correction factor η accounts for the non-Condon effect, and M is the geometric mean of the nuclear masses.[23] A typical level spacing of the final states d is used to estimate the density of final states, replacing the δ function in Fermi's golden rule.[20] The coefficients γ and δE in the exponent are typically obtained through experimental fitting (see eq S33).[20] For simplicity as well as computability, the assumptions of promoting modes (k_p) with zero Huang−Rhys factors and accepting modes (k_a) with nonzero Huang−Rhys factors are employed in the derivation of eq 4.[16,20,24] The promoting modes k_p, which have the largest J_{if}^k, make the main contribution to k_{NR},[25,26] and the remaining accepting modes k_a absorb the energy difference $\Delta E - \hbar\omega_{k_p}$,[20] where ω_{k_p} is the vibrational frequency of the promoting mode. For any promoting mode, energy conservation law dictates that $\Delta E = \hbar\omega_{k_p} + m_a\hbar\omega_{k_a}$, where $m_a = \sum_{k_a\neq k_p} m_{k_a}$ is the total vibrational quanta of all accepting modes. Assuming that there are p promoting modes, k_{NR} can eventually be expressed by eq 4 (see SI-3 and SI-4).

Equations 2 and 4 demonstrate that k_R depends mainly on the electronic coupling term, whereas k_{NR} is the product of two factors: the electronic coupling element and the Franck−Condon factor which is expressed as an exponential function. Historically, the Franck−Condon factor has been the focus of the evaluation of k_{NR}. In 1970, Freed et al. considered multiphonon processes in nonradiative decay[12] and proposed the commonly known energy gap law for k_{NR} in large molecules.[16] The energy gap law has been a widely utilized and convenient form for k_{NR}. It is noted that eq 4 is basically the same as that derived by Englman et al.[16] (see SI-4).

Schuurmans et al. investigated the correlation between J and J_{if}^k in rare earth atoms in a crystal and proposed a ratio between radiative and nonradiative decay rates under weak electron−phonon coupling conditions at low temperature.[20] For k_R, the operator in J acting on the electronic states is the electric dipole moment of the electrons ($\sum_e e\mathbf{r}_e$), while for k_{NR}, the operator in J_{if}^k is a first-order partial derivative with respect to the normal coordinates ($\partial/(\partial Q_k)$). To find the relationship between J and J_{if}^k, Schuurmans et al. employed the dipole moment expressed in the velocity form and acceleration form known as the Chandrasekhar relation.[27] In other words, J can be expressed in the velocity form

$$\langle\phi_f|\boldsymbol{\mu}|\phi_i\rangle_e = \frac{e\hbar^2}{m_e\Delta E}\left\langle\phi_f\left|\sum_e \nabla_{r_e}\right|\phi_i\right\rangle_e \quad (6)$$

m_e is the electron mass. The derivation of eq 6 employs the commutability between $\boldsymbol{\mu}$ and $V(\boldsymbol{r}, \boldsymbol{R})$. In view of the commutability of T_e with ∇_{r_e}, similarly it can be obtained that

https://doi.org/10.1021/acs.jpclett.3c00697
J. Phys. Chem. Lett. 2023, 14, 4151−4157

$$\left\langle \phi_f \left| \sum_e \nabla_{r_e} \right| \phi_i \right\rangle_e = \frac{1}{\Delta E} \left\langle \phi_f \left| \sum_e \nabla_{r_e} V(\boldsymbol{r}, \boldsymbol{R}) \right| \phi_i \right\rangle_e \tag{7}$$

T_e is the kinetic energy of the electron. Thus, one has the acceleration form:

$$\langle \phi_f | \boldsymbol{\mu} | \phi_i \rangle_e = \frac{e\hbar^2}{m_e \Delta E^2} \left\langle \phi_f \left| \sum_e \nabla_{r_e} V(\boldsymbol{r}, \boldsymbol{R}) \right| \phi_i \right\rangle_e \tag{8}$$

Correspondingly, J_{if}^k can also be transformed into its acceleration form as

$$\left\langle \phi_f \left| \sum_n \nabla_{R_n} \phi_i \right\rangle_e = \frac{1}{\Delta E} \left\langle \phi_f \left| \sum_n \nabla_{R_n} V(\boldsymbol{r}, \boldsymbol{R}) \right| \phi_i \right\rangle_e \tag{9}$$

The detailed derivations for eqs 6, 7, and 9 are given in the Supporting Information (see SI-5). In dealing with large fluorescent molecules, we use the single-electron approximation. Therefore, the interaction potential between particles ($V(\boldsymbol{r}, \boldsymbol{R})$) is mostly dominated by the Coulomb interaction (V_{en}) between the electron and the equivalent nucleus, resulting in $V(\boldsymbol{r}, \boldsymbol{R}) = V_{en}$. As a result, the interaction potential between particles satisfies

$$\sum_e \nabla_{r_e} V(\boldsymbol{r}, \boldsymbol{R}) + \sum_n \nabla_{R_n} V(\boldsymbol{r}, \boldsymbol{R}) = 0 \tag{10}$$

The single-electron approximation is important because it allows us to neglect the interaction potential energy between multielectrons (V_{ee}), without which eq 10 may not hold. Schuurmans et al. did not mention the use of a single-electron approximation in their work,[20] which makes their derivation of this part somewhat ambiguous. Moreover, eq 9 justifies the rationality of retaining the nonadiabatic Hamiltonian ΔH only to the first order since normally V_{en} is approximately linear to the deviation of the nuclei from its equilibrium position ($\boldsymbol{R} - \boldsymbol{R}^0$).[24,28,29] Combining eqs 7, 9, and 10 yields the following important relation:

$$\left\langle \phi_f \left| \sum_e \nabla_{r_e} \phi_i \right\rangle_e = -\left\langle \phi_f \left| \sum_n \nabla_{R_n} \phi_i \right\rangle_e \right. \tag{11}$$

This formula was proposed by Schuurmans et al. for the first time, and it indicates the "equivalence" of the gradient operator of electron coordinates and nuclear coordinates acting on the initial and final electronic states, when the interaction potential energy satisfies the symmetry condition in eq 10.[20]

By introducing an electronic interaction term $E_{an}(\boldsymbol{R}) = \left\langle \phi_f \left| \frac{\partial V(\boldsymbol{r}, \boldsymbol{R})}{\partial R_{an}} \right| \phi_i \right\rangle_e$, J can be expressed as $J = -\left(\frac{e\hbar^2}{m_e \Delta E^2}\right) \sum_{an} E_{an}(\boldsymbol{R})$. Here, the subscript an depicts Cartesian coordinate component (x, y, z) of the nucleus n. While $J_{if}^{k_p}$ in k_{NR} is based on normal coordinates Q_k, it can be transformed to the Cartesian coordinates R_{an} using the coordinate transformation relations between Q_k and R_{an} given by $R_{an} - R_{an}^0 = \sum_{k=1}^{3N} \sqrt{\frac{M}{M_n}} A_{an;k} Q_k$, where M_n is the mass of nucleus n and $A_{an;k}$ is the coordinate transformation matrix element (see SI-6). Then $J_{if}^{k_p}$ is written as $J_{if}^{k_p} = \frac{\left(\sum_{an} \sqrt{\frac{M}{M_n}} A_{an;k_p} E_{an}\right)}{\Delta E}$. In this way, both k_R and k_{NR} can be represented by E_{an}, and the ratio of these two rates at 0 K is given by

$$\frac{k_{NR}}{k_R} = \frac{3}{4} \frac{\pi \eta \hbar m_e^2 c^3}{e^2 \Delta E M} e^{\gamma(\Delta E + \delta E)} \sum_{k_p=1}^{p} C_{sym}^{k_p} \tag{12}$$

where

$$C_{sym}^{k_p} = \frac{\frac{\hbar \omega_{k_p}}{d} \left| \sum_{an} \sqrt{\frac{M}{M_n}} A_{an;k_p} E_{an} \right|^2}{\sum_a \left| \sum_n E_{an} \right|^2} \tag{13}$$

Therefore, a ratio of nonradiative and radiative decay rates at 0 K has been obtained by Schuurmans et al. This ratio, in the low-temperature limit, is an intrinsic constant that is challenging to confirm directly through experiments unless all of the relevant quantities can be calculated and are consistent with the experimentally measured rates.

Orlandi et al. proposed an electronic propensity rule that suggests a positive correlation between k_R and k_{NR} when the radiation field interacted with the electronic states.[18] Inspired by this electronic propensity rule, one feasible method to experimentally investigate the relationship between k_R and k_{NR} is to introduce a perturbation to the electronic transition potential by changing the external electric field without affecting the electronic transition spectrum and radiation spectrum. We examine the relationship between k_R and k_{NR} using the polarizable continuum model (PCM),[30−32] which considers the influence of the external electric field as a polar solution environment on the molecular system. PCM describes the surrounding solvent or nearby metal as a continuum medium, using apparent surface charges to estimate the electrostatic potential, and the property of the continuum medium is mainly described by the dielectric constant ε.[30−33] In the literature,[32] the apparent surface charges on the molecules induced by the external electric field $\boldsymbol{E}^{ex}$ are given by $q = AD^{-1}(\boldsymbol{E}^{ex} \cdot \boldsymbol{n})$, where $\boldsymbol{n}$ is the outward normal unit vector to the tesserae surface, D is a square matrix with size equal to the number of surface tesseras, and A is a square diagonal matrix having the same dimensions as D.[31,34] The external electric field of the solution environment can induce an additional transition dipole moment $\boldsymbol{\mu}'$, and then the total dipole moment is written as $\boldsymbol{\mu}_{tot} = \boldsymbol{\mu}_0 + \boldsymbol{\mu}'$.

The induced transition dipole moment is given as[31,32]

$$\boldsymbol{\mu}_j' = -\frac{\partial q}{\partial E_j^{ex}} V(\boldsymbol{r}, \boldsymbol{R}) = -(AD^{-1}\boldsymbol{n}_j) V(\boldsymbol{r}, \boldsymbol{R}) \tag{14}$$

When assuming molecules to be highly symmetrical and isotropic in solution, they can be treated as spheres with equivalent rotational diffusion coefficients and hydrodynamic radii in different directions.[31,35] In this study, we also assume a uniform apparent charge density distribution on the cavity surface and divide the surface into tesseras of equal area. In this way, the matrix D is symmetric and can be diagonalized to D', i.e., for spherical surfaces with uniform charge density $\boldsymbol{\mu}'_j = -(A_{jj} D'_{jj} \boldsymbol{n}_j) V(\boldsymbol{r}, \boldsymbol{R}) = \alpha V(\boldsymbol{r}, \boldsymbol{R}) \boldsymbol{n}_j$, where A_{jj} and D'_{jj} are the corresponding diagonal elements and α is related to the dielectric constant ε of the solution and the radius of the sphere.[31] According to eqs 6−10, the potential energy is related to the electric dipole moment via the relation $\langle \phi_f | \boldsymbol{\mu} | \phi_i \rangle_e$

https://doi.org/10.1021/acs.jpclett.3c00697
J. Phys. Chem. Lett. 2023, 14, 4151−4157

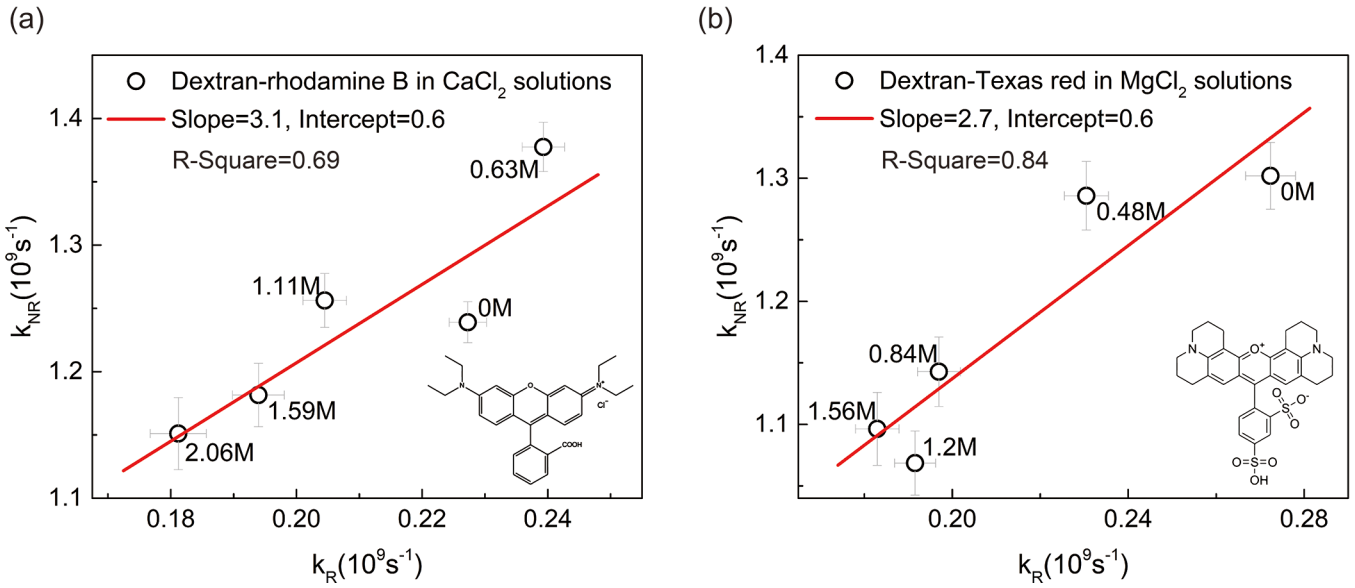

Figure 1. Plot of the calculated k_{NR} against k_R for (a) dextran−rhodamine B in $CaCl_2$ solutions with concentration ranging from 0 to 2.06 M and (b) dextran−Texas red in $MgCl_2$ solutions with concentration ranging from 0 to 1.56 M. The straight line on each plot represents the linear fit to the data.

$\propto \langle\phi_f|\sum_n \nabla_{R_n} V(\boldsymbol{r},\boldsymbol{R})|\phi_i\rangle$. When molecules are exposed to the electric field of the solution environment, the original potential energy $V(\boldsymbol{r}, \boldsymbol{R})$ is replaced by a new potential energy $V^{new}(\boldsymbol{r}, \boldsymbol{R}) = V(\boldsymbol{r}, \boldsymbol{R}) + \Delta V(\boldsymbol{r}, \boldsymbol{R})$, which means $\langle\phi_f|\boldsymbol{\mu}_{tot}|\phi_i\rangle_e \propto \langle\phi_f|\sum_n \nabla_{R_n} V^{new}(\boldsymbol{r}, \boldsymbol{R})|\phi_i\rangle$. Through $\boldsymbol{\mu}' = \sum_j (\boldsymbol{\mu}'_j \boldsymbol{n}_j)$, calculating the left-hand term of this formula gives

$$\begin{aligned}\langle\phi_f|\boldsymbol{\mu}_{tot}|\phi_i\rangle &= \langle\phi_f|\boldsymbol{\mu}_0|\phi_i\rangle + \langle\phi_f|\boldsymbol{\mu}'|\phi_i\rangle \\ &= \langle\phi_f|\boldsymbol{\mu}_0|\phi_i\rangle + \left\langle \phi_f \middle| \sum_{an} (\alpha V(\boldsymbol{r}, \boldsymbol{R}) n_{an}) \middle| \phi_i \right\rangle\end{aligned} \tag{15}$$

Evaluating the corresponding right-hand side gives

$$\begin{aligned}\left\langle \phi_f \middle| \sum_n \nabla_{R_n} V^{new}(\boldsymbol{r}, \boldsymbol{R}) \middle| \phi_i \right\rangle &= \left\langle \phi_f \middle| \sum_n \nabla_{R_n} (V(\boldsymbol{r}, \boldsymbol{R}) + \Delta V(\boldsymbol{r}, \boldsymbol{R})) \middle| \phi_i \right\rangle \\ &= \left\langle \phi_f \middle| \sum_n \nabla_{R_n} V(\boldsymbol{r}, \boldsymbol{R}) \middle| \phi_i \right\rangle + \left\langle \phi_f \middle| \sum_n \nabla_{R_n} (\Delta V(\boldsymbol{r}, \boldsymbol{R})) \middle| \phi_i \right\rangle\end{aligned} \tag{16}$$

By comparing eqs 15 and 16, with the relation between $\boldsymbol{\mu}_{tot}$ and $V^{new}(\boldsymbol{r}, \boldsymbol{R})$ above, we have

$$\left\langle \phi_f \middle| \sum_n \nabla_{R_n} \Delta V(\boldsymbol{r}, \boldsymbol{R}) \middle| \phi_i \right\rangle \propto \left\langle \phi_f \middle| \sum_{an} (\alpha V(\boldsymbol{r}, \boldsymbol{R}) \boldsymbol{n}_{an}) \middle| \phi_i \right\rangle \tag{17}$$

Correspondingly, the new electronic interaction term related to $V^{new}(\boldsymbol{r}, \boldsymbol{R})$ can be written as $E^{new}_{an}(\boldsymbol{R}) = E_{an}(\boldsymbol{R}) + \langle\phi_f|\alpha V(\boldsymbol{r}, \boldsymbol{R})|\phi_i\rangle_e$ (see SI-7). Obviously, the ratio of the electric field perturbation-induced term to E_{an}, i.e., $\frac{\langle\phi_f|\alpha V(\boldsymbol{r},\boldsymbol{R})|\phi_i\rangle_e}{E_{an}}$ denoted as β_{an}, is a constant for different "an" for the initial potential energy V_{en} of the system under consideration. Then we obtain $E^{new}_{an}(\boldsymbol{R}) = (1 + \beta_{an})E_{an}(\boldsymbol{R})$. By substituting $E^{new}_{an}(\boldsymbol{R})$ into eqs 12 and 13, it is evident that the ratio of k_{NR} to k_R is constant while their individual values vary with the dielectric constant ε of the external environment. Changing the dielectric constant (ε) of the solution can alter the values of both k_R and k_{NR} while maintaining their ratio invariant.

It should be noted that all of the above derivation is based on the low-temperature limit. Lin et al. have discussed the temperature dependence of k_{NR},[16,36,37] showing that the rate constant depends on temperature as $k_{NR}(T) = [1 + A(T)]k^0_{NR}$. They assumed that the temperature dependence of k_R will be similar to the above equation for nonradiative processes, which indicates $k_R(T) = [1 + B(T)]k^0_R$. Here k^0_{NR} and k^0_R are the rate constants at $T = 0$ K, while $A(T)$ and $B(T)$ are related to the vibrational modes.[36] Defining $\kappa^0 = (k^0_{NR})/(k^0_R)$, in higher temperature regions we have

$$k_{NR}(T) \approx \kappa^0 k_R(T) + \kappa^0[A(T) - B(T)] \times k^0_R \tag{18}$$

This illustrates that, under certain circumstances, $k_R(T)$ is linearly related to $k_{NR}(T)$ with a slope of κ^0, and the intercept is attributed to the temperature impact on the transition rates.

Experiments were conducted with two dye molecules conjugated to dextran, dextran−rhodamine B and dextran−Texas red, at room temperature to validate the theoretical linear relation. Dextran molecules were used as effective water-soluble carriers for the dyes due to their water solubility, low toxicity, and relative inertness. We measured the fluorescence quantum yield (Φ) and the excited-state lifetime (τ) of the two samples in solutions of $CaCl_2$ and $MgCl_2$ with different concentrations. The radiative and nonradiative decay rates were then calculated from the measured Φ and τ by $k_R = \Phi/\tau$ and $k_{NR} = (1 - \Phi)/\tau$.[2,19,38,39] The calculated k_{NR} and k_R of rhodamine B and Texas red are exhibited in Figure 1, where the linear relation holds.

The light-harvesting antenna complex (LH2) from *Rhodopseudomonas (Rps.) acidophila* consists of two concentric rings with a total of 27 bacteriochlorophyll *a* (BChl *a*) molecules, exhibiting high symmetry with a 9-fold rotational axis. The 2 rings named after their absorption bands are known as B800 with 9 BChl *a* molecules of larger interpigment separations and B850 with 18 BChl *a* molecules of shorter interpigment separations.[40,41] However, in solution, LH2 is distorted to an

https://doi.org/10.1021/acs.jpclett.3c00697
J. Phys. Chem. Lett. 2023, 14, 4151−4157

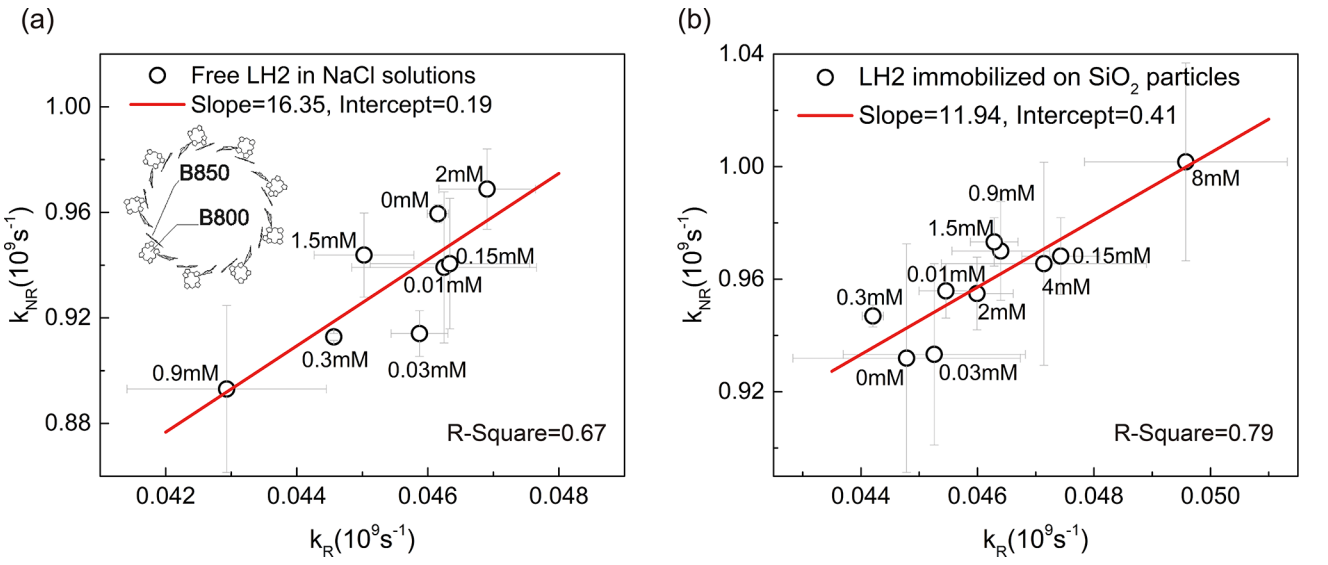

Figure 2. Correlation between k_{NR} and k_R of B850 fluorescence emission for (a) LH2 in NaCl solution with different concentrations and (b) LH2 adsorbed on 4 nm SiO_2 nanoparticles at different concentrations of NaCl. The straight line represents a linear fit in the concentration ranges of (a) 0 to 2 mM and (b) 0 to 8 mM.

elliptical structure.[42] Furthermore, the energy difference between the absorption and fluorescence peaks for the B850 ring is about 70 cm^{-1}, which indicates that LH2 is a weak coupling system.[43] In this work, we also determined k_{NR} and k_R of the B850 fluorescence band for free LH2 and LH2 immobilized on 4 nm SiO_2 nanoparticles in NaCl solutions with varying concentrations to further validate the theoretical linear relation at room temperature. The B850 excited state was prepared by an efficient energy transfer from B800 (>91%),[44] which can avoid the interference in the quantum yield measurement by direct excitation of B850. Figure 2 plots k_{NR} against k_R of free LH2 and LH2 immobilized on nanoparticles, which displays a linear relation when the concentration of NaCl changes since the dielectric constant ε of the solution changes accordingly.

In the above experiments, changes in the external electric field on the fluorescence molecules result from variations in salt concentration. As predicted, a linear relationship between k_{NR} and k_R was observed, as shown in Figures 1 and 2. Deviations from the theoretical linear relationship may be attributed to the temperature effect on the vibrational modes contributing to the Franck−Condon factor. Our theoretical work explores the influence of the external electric field perturbation on the electronic interaction part, assuming that the vibrational coupling part is unchanged. This assumption is valid under weak coupling, although experimental errors may still exist.

We have derived a linear relationship between the nonradiative and radiative decay rates for molecules under the weak coupling limit and a small perturbation from the external electric field at higher temperature. This provides an opportunity to experimentally verify the previously proposed electronic propensity rule by altering the environment of the molecules. The predicted linear relationship has been confirmed by our experimentally determined k_{NR} and k_R of rhodamine B and Texas red conjugated with dextran in $CaCl_2$ and $MgCl_2$ solutions, respectively. The calculated k_{NR} and k_R from B850 fluorescence emission for either free LH2 or LH2 immobilized on SiO_2 nanoparticles, where the external electric field variation was achieved by changing the NaCl concentration, also demonstrated a linear relationship.

The linear relationship proposed in our study relies on several assumptions and limitations, including (a) the weak electron−phonon coupling, where the extremely slight distortions and small displacements of the potential energy surfaces favor low-order perturbation processes for nonradiative decay and the adiabatic approximation and harmonic approximation naturally hold; (b) the single-electron approximation, where the interaction potential between particles is approximated as the electrostatic potential of an electron and the equivalent nucleus, satisfying eq 10; (c) the temperature-dependent relation for rates of the form $k(T) = [1 + A(T)]k^0$; (d) the stable and symmetrical structure of molecules, which ensures that the molecule can be treated as a spherical cavity with uniform surface charge; and (e) a weak external electric field relative to the electrostatic interactions inside the molecule, allowing the original electronic-state manifold of the molecule to be maintained.

Sample preparations of dextran−rhodamine B (10 000 MW, neutral) and dextran−Texas red (3000 MW, neutral) were purchased from Thermo Fisher Scientific. Dextran−rhodamine B and dextran−Texas red were dissolved in solutions of $CaCl_2$ and $MgCl_2$ with varying concentrations. The preparation and purification of LH2 complexes and the assembling of LH2 onto the SiO_2 nanoparticles have been reported in ref 45. Different concentrations of NaCl were added to the LH2 and LH2/SiO_2 solutions.

The lifetimes (τ) of LH2 and LH2/SiO_2 were measured with a femtosecond time-resolved difference absorbance spectrometer under 800 nm excitation. The standard deviation was calculated from three individual measurements. The details of this method have been described elsewhere.[45−47] For the dextran−dye complexes, we used time-resolved fluorescence measurements with a streak camera. Samples were placed into a 1-mm-thick fused silica cuvette with an optical density of 0.134 at 570 nm for dextran−rhodamine B and 0.123 at 595 nm for dextran−Texas red. A femtosecond amplifier (Spectra Physics, USA) delivered a 70 fs pulse at a

https://doi.org/10.1021/acs.jpclett.3c00697
J. Phys. Chem. Lett. 2023, 14, 4151−4157

repetition rate of 5 kHz. Excitation light (530 and 558 nm) generated from a commercialized tunable optical parametric amplification system (TOPAS, Spectra Physics) pumped by the femtosecond amplifier was used to excite rhodamine B and Texas red, respectively. A pulse energy of 5 nJ per pulse with a spot size of ∼50 μm was used to excite the sample. A high-quality 600 nm long-pass band filter was used to block the residual excitation pulse. The emitted fluorescence was collected and focused into a spectrograph and measured with a 5200 (XIOPM, China) streak camera operating in the 1.4 ns scanning range with a time resolution of ∼40 ps. The spectral window recorded by the CCD of the streak camera was 260 nm in the measurements, covering the fluorescence wavelength of dye samples. The time-resolved fluorescence data were averaged over 10 single measurements, and the kinetics corresponding to the wavelength of the fluorescence peak were selected to obtain the fluorescence lifetime of the sample.

The fluorescence quantum yield (Φ) was measured with the absolute photoluminescence quantum spectrometer (C11347, Hamamatsu Photonics) under 800 nm excitation for LH2 and LH2/SiO_2, 560 nm excitation for dextran−rhodamine B, and 580 nm excitation for dextran−Texas red.

■ ASSOCIATED CONTENT

Supporting Information

The Supporting Information is available free of charge at https://pubs.acs.org/doi/10.1021/acs.jpclett.3c00697.

Some detailed additions to the theoretical derivation (PDF)

■ AUTHOR INFORMATION

Corresponding Author

Yuxiang Weng − *Laboratory of Soft Matter Physics, Institute of Physics, Chinese Academy of Sciences, Beijing 100190, China; University of Chinese Academy of Sciences, Beijing 100049, China; Songshan Lake Materials Laboratory, Dongguan, Guangdong 523808, China;* orcid.org/0000-0003-0423-2266; Email: yxweng@iphy.ac.cn

Authors

Ying Zhang − *Laboratory of Soft Matter Physics, Institute of Physics, Chinese Academy of Sciences, Beijing 100190, China; University of Chinese Academy of Sciences, Beijing 100049, China;* orcid.org/0000-0003-2527-9397

Heyuan Liu − *Laboratory of Soft Matter Physics, Institute of Physics, Chinese Academy of Sciences, Beijing 100190, China; University of Chinese Academy of Sciences, Beijing 100049, China*

Complete contact information is available at: https://pubs.acs.org/10.1021/acs.jpclett.3c00697

Notes

The authors declare no competing financial interest.

■ ACKNOWLEDGMENTS

The authors thank the Ministry of Science and Technology (2018YFA0208700), the National Natural Science Foundation of China (22027802, 11721404), the Strategic Priority Research Program of the Chinese Academy of Sciences (XDB33000000), and the Chinese Academy of Sciences Frontier Science Key Programs (QYZDJ-SSW-SYS017) for financial support.

■ REFERENCES

(1) Wei, Y.-C.; Wang, S.-F.; Hu, Y.; Liao, L.-S.; Chen, D.-G.; Chang, K.-H.; Wang, C.-W.; Liu, S.-H.; Chan, W.-H.; Liao, J.-L.; et al. Overcoming the Energy Gap Law in Near-Infrared OLEDs by Exciton−Vibration Decoupling. *Nat. Photonics* **2020**, *14*, 570−577.

(2) Hoche, J.; Schulz, A.; Dietrich, L. M.; Humeniuk, A.; Stolte, M.; Schmidt, D.; Brixner, T.; Würthner, F.; Mitric, R. The Origin of the Solvent Dependence of Fluorescence Quantum Yields in Dipolar Merocyanine Dyes. *Chem. Sci.* **2019**, *10*, 11013−11022.

(3) Friedman, H. C.; Cosco, E. D.; Atallah, T. L.; Jia, S.; Sletten, E. M.; Caram, J. R. Establishing Design Principles for Emissive Organic SWIR Chromophores from Energy Gap Laws. *Chem.* **2021**, *7*, 3359−3376.

(4) Valiev, R. R.; Cherepanov, V. N.; Baryshnikov, G. V.; Sundholm, D. First-Principles Method for Calculating the Rate Constants of Internal-Conversion and Intersystem-Crossing Transitions. *Phys. Chem. Chem. Phys.* **2018**, *20*, 6121−6133.

(5) Guan, J.; Shen, C.; Peng, J.; Zheng, J. What Leads to Aggregation-Induced Emission? *J. Phys. Chem. Lett.* **2021**, *12*, 4218−4226.

(6) Li, W.; Peng, Q.; Xie, Y.; Zhang, T.; Shuai, Z. Effect of Intermolecular Excited-State Interaction on Vibrationally Resolved Optical Spectra in Organic Molecular Aggregates. *Acta Chim. Sinica* **2016**, *74*, 902−909.

(7) Peng, Q.; Shuai, Z. Molecular Mechanism of Aggregation-Induced Emission. *Aggregate* **2021**, *2*, e91.

(8) Heitler, W. *The Quantum Theory of Radiation*; Oxford University Press, 1954.

(9) Scully, M. O.; Zubairy, M. S. *Quantum Optics*; Cambridge University Press, 1997.

(10) Lin, S. H. Rate of Interconversion of Electronic and Vibrational Energy. *J. Chem. Phys.* **1966**, *44*, 3759−3767.

(11) Siebrand, W. Radiationless Transitions in Polyatomic Molecules. I. Calculation of Franck-Condon Factors. *J. Chem. Phys.* **1967**, *46*, 440−447.

(12) Freed, K. F.; Jortner, J. Multiphonon Processes in the Nonradiative Decay of Large Molecules. *J. Chem. Phys.* **1970**, *52*, 6272−6291.

(13) Lin, S. H. Energy Gap Law and Franck-Condon Factor in Radiationless Transitions. *J. Chem. Phys.* **1970**, *53*, 3766−3767.

(14) Lin, S. H.; Eyring, H. Quantum Statistical Theory of Rate Processes. *Proc. Natl. Acad. Sci. U. S. A.* **1972**, *69*, 3192−3194.

(15) Bondybey, V. E.; Nitzan, A. Radiationless Transitions in Small Molecules: Interstate Cascading in Matrix-Isolated CN. *Phys. Rev. Lett.* **1977**, *38*, 889−892.

(16) Englman, R.; Jortner, J. The Energy Gap Law for Radiationless Transitions in Large Molecules. *Mol. Phys.* **1970**, *18*, 145−164.

(17) Wessner, J. M.; Anderson, D. K.; Robiscoe, R. T. Radiative Decay of the 2P State of Atomic Hydrogen: A Test of the Exponential Decay Law. *Phys. Rev. Lett.* **1972**, *29*, 1126−1128.

(18) Orlandi, G.; Siebrand, W. Electronic Propensity Rule for Radiationless Transitions. *Chem. Phys. Lett.* **1981**, *80*, 399−403.

(19) Lim, B. T.; Lin, S. H.; Lim, E. C. Interdependence of Radiative and Nonradiatibe Decay Rates of the Lowest Excited Singlet State as Revealed by the Fluorescence of Dinaphthylalkanes. *J. Chem. Phys.* **1983**, *78*, 1112−1116.

(20) Schuurmans, M. F. H.; van Dijk, J. M. F. On Radiative and Non-Radiative Decay Times in the Weak Coupling Limit. *Physica B & C* **1984**, *123*, 131−155.

(21) van Dijk, J. M. F.; Schuurmans, M. F. H. On the Nonradiative and Radiative Decay Rates and a Modified Exponential Energy-Gap Law for 4f-4f Transitions in Rare-Earth Ions. *J. Chem. Phys.* **1983**, *78*, 5317−5323.

(22) Strickler, S. J.; Berg, R. A. Relationship between Absorption Intensity and Fluorescence Lifetime of Molecules. *J. Chem. Phys.* **1962**, *37*, 814−822.

(23) Nitzan, A.; Jortner, J. Radiationless Decay and Intrastate Energy Equilibration in an Isolated Large Molecule. *J. Chem. Phys.* **1972**, *56*, 5200−5201.

(24) Huang, K.; Rhys, A. Theory of Light Absorption and Non-Radiative Transitions in F-Centres. *Proc. R. Soc. A* **1950**, *204*, 406−423.
(25) Niu, Y.; Peng, Q.; Shuai, Z. Promoting-Mode Free Formalism for Excited State Radiationless Decay Process with Duschinsky Rotation Effect. *Sci. China Ser. B-Chem.* **2008**, *51*, 1153−1158.
(26) Rice, S. A. Overview of Some Quantum Effects in Chemistry. *Procedia Chem.* **2011**, *3*, 17−32.
(27) Chandrasekhar, S. On the Continuous Absorption Coefficient of the Negative Hydrogen Ion. *Astrophys. J.* **1945**, *102*, 223−231.
(28) Gummel, H.; Lax, M. Thermal Capture of Electrons in Silicon. *Ann. Phys.* **1957**, *2*, 28−56.
(29) Ram, M. Radiative Decay-Rate Relation for Isobaric Multiplets. *Phys. Rev. Lett.* **1970**, *25*, 391−393.
(30) Miertuš, S.; Scrocco, E.; Tomasi, J. Electrostatic Interaction of a Solute with a Continuum. A Direct Utilization of AB Initio Molecular Potentials for the Prevision of Solvent Effects. *Chem. Phys.* **1981**, *55*, 117−129.
(31) Cammi, R.; Tomasi, J. Remarks on the Use of the Apparent Surface Charges (ASC) Methods in Solvation Problems: Iterative versus Matrix-Inversion Procedures and the Renormalization of the Apparent Charges. *J. Comput. Chem.* **1995**, *16*, 1449−1458.
(32) Andreussi, O.; Corni, S.; Mennucci, B.; Tomasi, J. Radiative and Nonradiative Decay Rates of a Molecule Close to a Metal Particle of Complex Shape. *J. Chem. Phys.* **2004**, *121*, 10190−10202.
(33) Berman, P. R.; Milonni, P. W. Microscopic Theory of Modified Spontaneous Emission in a Dielectric. *Phys. Rev. Lett.* **2004**, *92*, 053601.
(34) Corni, S.; Tomasi, J. Enhanced Response Properties of a Chromophore Physisorbed on a Metal Particle. *J. Chem. Phys.* **2001**, *114*, 3739−3751.
(35) Loman, A.; Gregor, I.; Stutz, C.; Mund, M.; Enderlein, J. Measuring Rotational Diffusion of Macromolecules by Fluorescence Correlation Spectroscopy. *Photochem. Photobiol. Sci.* **2010**, *9*, 627−636.
(36) Lin, S. H. Effect of Temperature on Radiationless Transitions. *J. Chem. Phys.* **1972**, *56*, 2648−2653.
(37) Sturge, M. D. Temperature Dependence of Multiphonon Nonradiative Decay at an Isolated Impurity Center. *Phys. Rev. B* **1973**, *8*, 6−14.
(38) Kelly, L. A.; Roll, M.; Joseph, J.; Seenisamy, J.; Barrett, J.; Kauser, K.; Warner, K. S. Solvent-Dependent Photophysics and Reactivity of Monomeric and Dimeric 4-Amino-1,8-Naphthalimides. *J. Phys. Chem. A* **2021**, *125*, 2294−2307.
(39) Brokmann, X.; Coolen, L.; Dahan, M.; Hermier, J. P. Measurement of the Radiative and Nonradiative Decay Rates of Single CdSe Nanocrystals through a Controlled Modification of their Spontaneous Emission. *Phys. Rev. Lett.* **2004**, *93*, 107403.
(40) McDermott, G.; Prince, S. M.; Freer, A. A.; Hawthornthwaite-Lawless, A. M.; Papiz, M. Z.; Cogdell, R. J.; Isaacs, N. W. Crystal Structure of an Integral Membrane Light-Harvesting Complex from Photosynthetic Bacteria. *Nature* **1995**, *374*, 517−521.
(41) Papiz, M. Z.; Prince, S. M.; Howard, T.; Cogdell, R. J.; Isaacs, N. W. The Structure and Thermal Motion of the B800−850 LH2 Complex from Rps. acidophila at 2.0Å Resolution and 100K: New Structural Features and Functionally Relevant Motions. *J. Mol. Biol.* **2003**, *326*, 1523−1538.
(42) Hong, X.; Weng, Y.-X.; Li, M. Determination of the Topological Shape of Integral Membrane Protein Light-Harvesting Complex LH2 from Photosynthetic Bacteria in the Detergent Solution by Small-Angle X-Ray Scattering. *Biophys. J.* **2004**, *86*, 1082−1088.
(43) Horák, M.; Herman, P.; Zapletal, D. Modeling of Emission Spectra for Molecular Rings - LH2 and LH4 Complexes. *Phys. Procedia* **2013**, *44*, 10−18.
(44) Papagiannakis, E.; Kennis, J. T. M.; van Stokkum, I. H. M.; Cogdell, R. J.; van Grondelle, R. An Alternative Carotenoid-to-Bacteriochlorophyll Energy Transfer Pathway in Photosynthetic Light Harvesting. *Proc. Natl. Acad. Sci. U. S. A.* **2002**, *99*, 6017−6022.
(45) Chen, X.-H.; Zhang, L.; Weng, Y.-X.; Du, L.-C.; Ye, M.-P.; Yang, G.-Z.; Fujii, R.; Rondonuwu, F. S.; Koyama, Y.; Wu, Y.-S.; et al. Protein Structural Deformation Induced Lifetime Shortening of Photosynthetic Bacteria Light-Harvesting Complex LH2 Excited State. *Biophys. J.* **2005**, *88*, 4262−4273.
(46) Du, L.-C.; Huang, Y.-F.; Ren, B.; Weng, Y.-X. Photosynthetic Bacterial Light-Harvesting Antenna Complexes Adsorbed on Silica Nanoparticles Revealed by Silica Shell-Isolated Au Nanoparticle-Enhanced Raman Spectroscopy. *J. Phys. Chem. C* **2012**, *116*, 6993−6999.
(47) Shi, Y.-R.; Ye, M.-P.; Du, L.-C.; Weng, Y.-X. Experimental Determination of Particle Size-Dependent Surface Charge Density for Silica Nanospheres. *J. Phys. Chem. C* **2018**, *122*, 23764−23771.

https://doi.org/10.1021/acs.jpclett.3c00697
J. Phys. Chem. Lett. 2023, 14, 4151−4157